metals

MDPI

Article

Efficient Recovery of High-Purity Li_2CO_3 from Spent Li-$SOCl_2$ Primary Batteries Through Thermal Treatment and Selective Hydrometallurgical Processing

Lorena Alcaraz *, Olga Rodríguez-Largo and Félix A. López

Centro Nacional de Investigaciones Metalúrgicas (CENIM), Consejo Superior de Investigaciones Científicas (CSIC), Avenida Gregorio del Amo 8, 28040 Madrid, Spain; olga.rodriguez@csic.es (O.R.-L.); f.lopez@csic.es (F.A.L.)

* Correspondence: alcaraz@cenim.csic.es

Abstract

Lithium-thionyl chloride (Li-$SOCl_2$) primary batteries contain a large amount of lithium and are increasingly being produced as hazardous waste, but little work has been done on recycling these batteries. This study reports an efficient process for the recycling of Li from used Li-$SOCl_2$ batteries using thermal treatment, water leaching and selective precipitation. The recovered black mass obtained after manual dismantling of the batteries contained 6.734 wt.% Li, which was thermally treated under different conditions to minimize lithium loss. Thermal treatment at 500 °C for 2 h limited Li volatilization to about 7%, but loss was significant at higher temperatures. Water leaching selectively recovered lithium into solution, leaving most of the impurities in the solid residue. Different precipitation strategies were assessed for the recovery of lithium as Li_2CO_3. Although ammonium carbonate yielded a recovery efficiency at 68%, sodium carbonate provided higher overall precipitation yields. Thus, the optimal conditions involved solution preconcentration, pH adjustment to above 11, and the use of ethanol as an antisolvent using sodium carbonate as a precipitating agent. These results reveal an efficient recycling pathway to recover lithium from spent Li-$SOCl_2$ batteries, contributing to the sustainable management of this under-explored battery waste stream.

Keywords: Li-$SOCl_2$ batteries; primary lithium-ion batteries; lithium recovery; battery recycling

Academic Editor: Petros E. Tsakiridis

Received: 2 September 2026
Revised: 15 September 2026
Accepted: 16 September 2026
Published: 18 September 2026

1. Introduction

Lithium is a critical raw material widely used in the manufacture of rechargeable lithium-ion batteries, which are essential for portable electronics devices, electric vehicles, and renewable energy storage systems [1]. However, the increasing global demand for lithium is exerting significant pressure on natural reserves, most of which are concentrated in a few geographic regions, such as the "Lithium Triangle" in South America [2,3]. This growing demand, coupled with geopolitical and environmental challenges associated with primary extraction, has raised concerns about the long-term availability and sustainability of lithium supplies [4]. In this context, the recovery of lithium from secondary sources, including spent and/or end-of-life batteries, has been identified as a strategic approach to the problems related to limited lithium reserves, reduced environmental impact from mining, and support for the establishment of a circular economy [5–7]. Lithium-ion batteries can be classified into primary (non-rechargeable) and secondary (rechargeable), each with different characteristics

and applications. Primary lithium batteries use metallic lithium as the anode and provide high energy density and very low self-discharge rates. Lithium metal, with its extremely low density (6.941 g mol^{-1}, 0.534 g cm^{-3}) and the most negative electrochemical potential (−3.04 V vs. SHE), enables lithium primary batteries to deliver a high energy density and a broad voltage window [8]. This makes them suitable for long-duration and low-power applications like medical implants and military equipment, among others. However, primary lithium batteries have the disadvantage of being one-time use only, carry significant safety risks due to the presence of reactive lithium metal, and present environmental challenges due to limited recyclability. In contrast, secondary lithium batteries are designed to be rechargeable, providing high energy and very long cycle life, along with numerous versatile applications, such as portable electronics, electric vehicles, and grid storage [9,10].

Among the primary batteries, Li-$SOCl_2$ batteries have been successfully commercialized and currently offer the highest specific energy. This battery technology offers substantial benefits, including an ultra-high cell-level energy density of 700 Wh kg^{-1}, a remarkably broad operating temperature range (−120 to 150 °C), and a high discharge voltage plateau exceeding 3.3 V. Furthermore, they feature a minimal self-discharge rate of approximately 1% per year and an exceptional storage life of over 15 years [8].

While secondary batteries offer better sustainability and recycling prospects, both technologies face challenges in material sourcing, environmental impact, and lifecycle management, prompting continued research into solid-state batteries, greener chemistries, and circular design principles [9].

Since these batteries are designed for single use, they pose a significant environmental threat if they are improperly discarded. They reach their end of life in landfills, and the corrosion of their metal casings can cause heavy metals and toxic chemical compounds to leach into the environment, leading to degraded soil quality and contaminated groundwater. Consequently, the EPA (Environmental Protection Agency) classifies them as hazardous waste due to their high inflammability and reactivity (under codes D001 and D003) [11], necessitating proper management of this waste and recycling protocols.

Despite the extensive literature on lithium recovery from lithium-ion batteries, recycling studies focused on primary Li-$SOCl_2$ batteries are extremely scarce [12]. Consequently, the development of dedicated recycling routes for this waste stream represents an important research challenge. The presence of solid lithium salts offers a promising basis for applying hydrometallurgical or mechanochemical recovery techniques—methods already proven effective in the recycling of lithium-ion batteries.

Among primary lithium batteries, lithium-thionyl chloride (Li/$SOCl_2$) systems exhibit exceptionally high energy densities, long shelf lives, and reliability, making them ideal for several applications. Lithium-thionyl chloride (Li/$SOCl_2$) batteries function through an electrochemical reaction between a lithium anode and a thionyl chloride cathode. In these types of batteries, the electrolyte also acts as the active cathode material. The discharge process involves lithium oxidation at the anode and thionyl chloride reduction at the cathode, producing lithium chloride, sulfur, and sulfur dioxide, while a passivating layer of LiCl forms on the lithium anode [13], as shown in Equations (1) and (2). The generated sulfur dioxide dissolves in excess thionyl chloride electrolyte.

$$\text{Negative electrode}: \ 4Li - 4e^- \rightarrow 4Li^+ \quad (1)$$

$$\text{Positive electrode}: \ 2SOCl_2 + 4e^- \rightarrow 4Cl^- \quad (2)$$

This study demonstrates the feasibility of recovering lithium from spent Li-$SOCl_2$ batteries through a combined pyrometallurgical and hydrometallurgical process. The first stage involves thermal treatment of the black mass at low temperatures, effectively decom-

posing lithium-containing compounds into more reactive forms. Subsequently, aqueous leaching enables the selective dissolution of lithium into solution while minimizing the co-dissolution of other metallic species. The final recovery step involves selective precipitation of lithium as lithium carbonate (Li_2CO_3) to achieve high purity and yield. This integrated process shows promising efficiency for lithium recovery from primary lithium-thionyl chloride batteries, offering a potential route for closing the loop on this underexplored battery chemistry and contributing to resource sustainability in the battery sector.

2. Materials and Methods

2.1. Dismantling of the Batteries and Obtaining the Black Mass

Two different types of Li-$SOCl_2$ batteries (FANSO ER26500H+1SPC 1550 and FANSO ER26500H+2SPC 1550, see Figure 1) were provided by TST Sistemas (Santander, Cantabria, España). These are high-capacity energy packs that combine a primary lithium cell (ER26500H) with one (SPC1550) or two pulse capacitors (2SPC 1550). These batteries were manually dismantled, and each component was separated.

Figure 1. FANSO ER26500H+1SPC 1550 and FANSO ER26500H+2SPC 1550 batteries used in the present work.

Li-$SOCl_2$ batteries usually consist of a stainless steel shell, a separator generally composed of a fiberglass membrane, an electrolyte normally composed of $SOCl_2$ solvent with inorganic salts such as $LiClO_4$ or $LiAlCl_4$, a metallic Li anode, and a porous carbon cathode host with $SOCl_2$ as the active material. $SOCl_2$ is loaded into the porous carbon through physical adsorption. As a result, $SOCl_2$ simultaneously functions as the solvent, an electrolyte component, and the cathode active material [8].

According to the model proposed by Schlaikjer et al. [14], the overall reaction in a Li-$SOCl_2$ primary battery can be expressed according to Equation (3):

$$4Li + 2SOCl_2 \rightarrow S + SO_2 + 4LiCl \quad (3)$$

During the discharge of a Li-$SOCl_2$ battery, the electrochemical process produces LiCl and elemental sulfur as solid products, which precipitate on the carbon cathodes [15].

Previously discharged batteries were manually dismantled under controlled conditions to minimize risks associated with exposure to active chemical compounds, short circuits, or battery explosion.

Initially, a set of cells (three for the ER26500H+2SPC 1550 batteries, two large and one small, and two for the ER26500H+1SPC 1550 batteries, one large and one small) connected and enclosed in a plastic casing were observed. Cutting tools were used to remove the external plastic covering. Subsequently, the individual cells were separated, and their metallic casings were removed, allowing access to the internal components of each cell. Once the cell housing was opened, internal components, such as plastic separators, insulating disks, and metal covers were extracted. Finally, the cell core was carefully unrolled, revealing a multilayered sheet composed of electrodes (anode and cathode) and the separator.

As illustrated in Figure 2, the $LiSOCl_2$ batteries were mainly composed of metals (Figure 2a), plastics (Figure 2b,c), and black mass (Figure 2d).

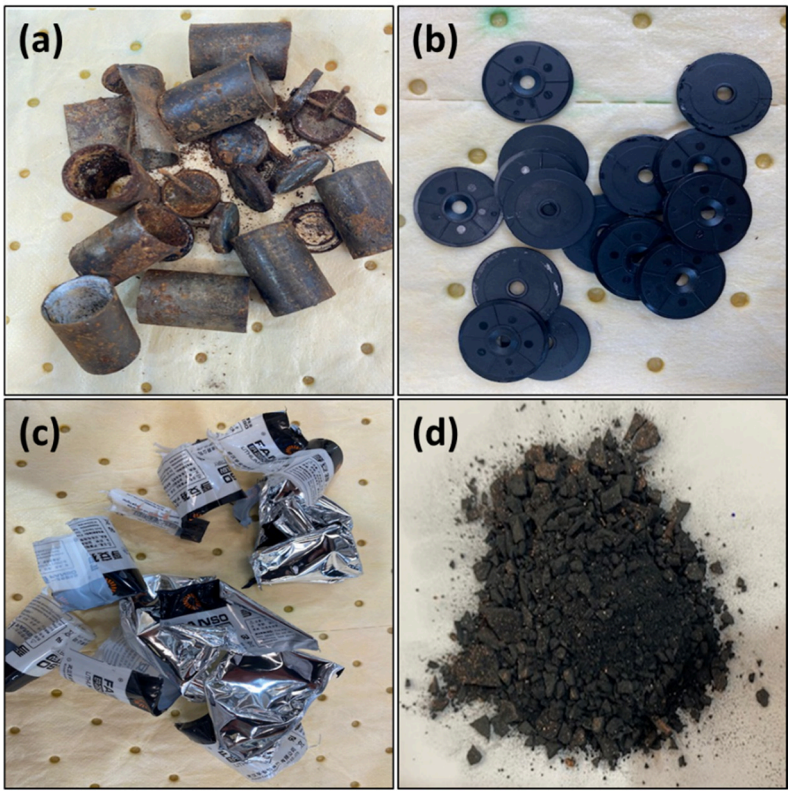

Figure 2. Different components obtained from the dismantling of Li-$SOCl_2$ batteries include metals (**a**), plastics (**b**,**c**), and recovered black mass (**d**).

Figure 3 exhibits the material compositions of the two types of batteries. In the case of the ER26500H+2SPC1550 batteries, metals represented the highest fraction (60.62%), followed by black mass (14.69%), anode (7.73%), and cathode (6.27%). For the ER26500H+1SPC1550 batteries, metals also dominated (58.97%), with significant contributions from the anode (11.49%) and cathode (9.32%). Plastics, adhesives, copper wire, and cellulose accounted for smaller fractions in both types of batteries.

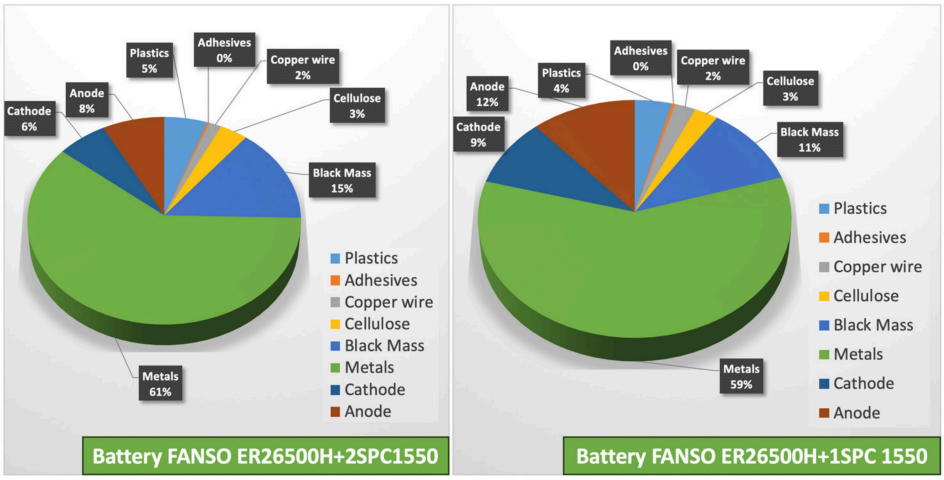

Figure 3. Weight percentage distribution of the components in FANSO ER26500H and ER26500H+15PC 1550 batteries.

Therefore, the black mass recovered from both types of batteries was used as the starting material for subsequent experiments.

2.2. Characterization

The metal content in the solutions obtained was analyzed by Inductively Coupled Plasma–Optical Emission Spectrometry (ICP-OES) using an Agilent ICP-OES (Agilent Technologies, Santa Clara, CA, USA), model 5100 VDV (Vertical Dual View).

The composition of the powders was determined through digestion of the solids. First, 1 g of each sample was treated with aqua regia and subjected to heating for the previously determined time. The liquid volume for each test was kept constant. Finally, the mixture was transferred to a 100 mL flask and brought to volume using MilliQ water (Merck KGaA, Darmstadt, Germany).

Structural characterization was carried out via X-ray diffraction (XRD) using an X'Pert Pro MPD diffractometer (PANalytical, Almelo, The Netherlands) equipped with a Cu anode (Cu Kα radiation) with a step size of 0.03° (2θ) in the range of 10–90°.

The morphology of the samples was analyzed by field emission scanning electron microscopy (FE-SEM) using a JEOL JSM-IT700HR microscope (JEOL Ltd., Tokyo, Japan), with an energy-dispersive X-ray microanalyzer (EDX). For SEM observations, the powder samples were placed on an adhesive conductive carbon disk.

3. Results and Discussion

3.1. Characterization of the Starting Black Mass

The chemical composition of the recovered black mass, measured by ICP-OES, is summarized in Table 1. The lithium content was quantified as 6.734 wt.%, whereas the levels of other elements were comparatively low. Only a similar sulfur content was detected, as expected in the composition of this type of battery.

Table 1. Chemical composition of the starting black mass.

Element	wt.%
Al	0.979
B	0.002
Ba	<LD
Bi	<LD
Ca	0.009
Cd	<LD
Co	0.058
Cr	0.013
Cu	0.648
Fe	0.061
K	<LD
Li	6.734
Mg	0.001
Mn	0.048
Mo	<LD
Na	0.006
Ni	0.388
P	0.022
Pb	<LD
S	5.510
Sb	<0.001
Si	0.020
Sn	0.010

Table 1. *Cont.*

Element	wt.%
Sr	0.001
Ta	<LD
Ti	0.002
V	<LD
Zn	0.008

LD: Limit of detection.

The XRD pattern and SEM images (Figure 4) reveal a semi-crystalline structure characterized by a prominent amorphous background, alongside some well-defined diffraction peaks, indicating the presence of at least one crystalline phase in the sample. This behavior is likely attributable to a high content of disordered carbonaceous material. Additionally, the EDX spectrum (Figure 4b inset) confirms the elemental composition of the sample, showing a predominant carbon matrix with only trace amounts of sulfur.

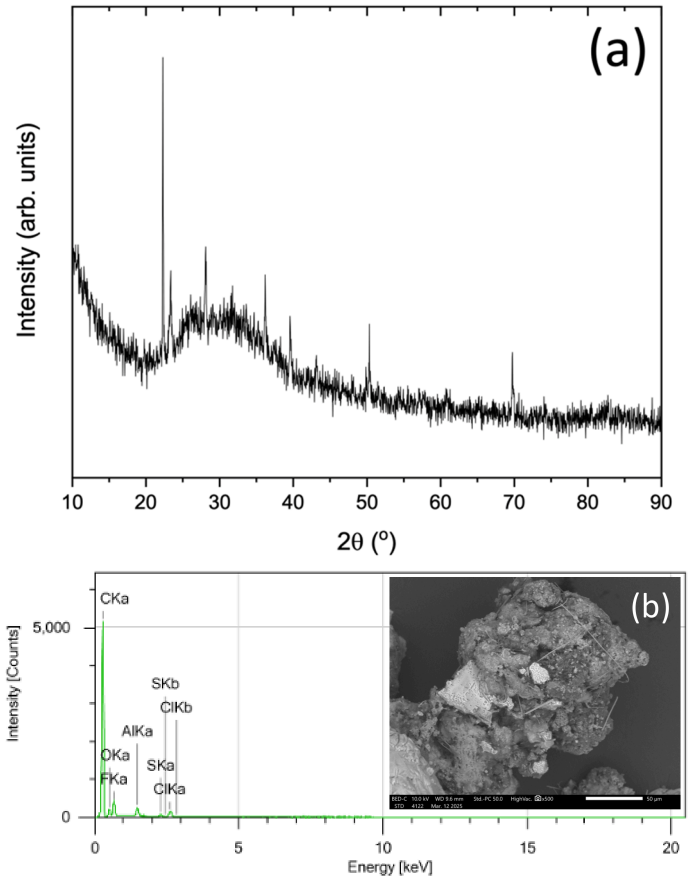

Figure 4. (**a**) XRD pattern for the starting black mass, and (**b**) SEM image and EDX analysis.

3.2. Thermal Treatment of the Black Mass

Given the significant lithium content detected in the black mass, further processing steps will be undertaken to recover the lithium. These subsequent treatments aim to separate and recover lithium from the remaining matrix through metallurgical methods.

To the best of our knowledge, research on lithium recovery from Li-$SOCl_2$ batteries is limited. In the present work, lithium recovery from the obtained black mass was investigated based on lithium recovery processes from other types of black masses. The overall process consists of a thermal treatment step, followed by a hydrolysis step [16].

For the thermal treatment, a homogeneous mixture of black mass and carbon black as the reducing agent (20 wt.%) was placed in an alumina crucible. N_2 flow was used to maintain an inert atmosphere while the mixture was heated in the furnace at a set temperature. Several conditions were assessed to analyze the influence of the thermal treatment.

Table 2 summarizes the thermal treatment conditions employed, along with the amount of Li lost. It should be noted that lithium loss was determined by comparing the lithium amount in the mixture before and after the thermal treatment after digestion of the corresponding solids. As shown, the combination of high temperatures and prolonged thermal treatment resulted in significant Li loss (test 1). A similar trend was observed when the thermal treatment was carried out at short times at elevated temperatures (test 2).

Table 2. Experimental conditions used in the thermal treatment process, and lithium and mass loss in each of them.

Thermal Treatment Test	Temperature (°C)	Reaction Time (h)	Li Loss (%)	Mass Loss (%)
1	850	4	48	60
2	850	1	35	39
3	500	2	7	13

These results can be attributed to the increased vapor pressure of lithium-containing species at elevated temperatures [17]. Unlike conventional lithium-ion batteries, where lithium is strongly bound within complex transition metal oxide frameworks, the black mass from Li-$SOCl_2$ batteries contains lithium predominantly as LiCl, which is generated during battery discharge. Although the boiling point of LiCl is substantially higher than the temperatures investigated in this study, volatilization can occur well below the boiling temperature because vapor pressure increases continuously with temperature and may become significant even in the solid state. Consequently, prolonged thermal treatment at 850 °C promotes lithium loss through volatilization, whereas operation at 500 °C effectively limits this phenomenon. Furthermore, the complex chemical composition of the black mass may lead to the formation of volatile lithium-containing species during thermal treatment, making the overall volatilization behavior more complex than that of pure LiCl alone. Therefore, careful optimization of the treatment temperature is essential to maximize lithium retention while ensuring the decomposition of sulfur-containing compounds.

The first stage involves a thermal treatment of the black mass at moderate temperatures. Temperature optimization is particularly important because lithium loss may occur through volatilization of lithium-containing species during thermal processing.

After the carboreduction tests, the thermally treated black mass mixture was subjected to a hydrolysis step at room temperature for 2 h with constant mechanical stirring. Subsequently, the final suspension was filtered, and each fraction was analyzed independently. A comparison of the chemical compositions of the carboreduced and the water-leached carboreduced black mass is exhibited in Table 3. While the lithium content in the thermally treated black mass was measured by ICP-OES at 6.29 wt.%, this value decreased significantly to 1.43 wt.% following the water-leaching step, demonstrating the high efficiency of the process.

In addition, the XRD pattern (Figure 5a) of the solid fraction reveals a predominantly amorphous carbon graphite structure, where some crystalline reflections can be observed, attributable to sulfur phase [card nº 01-089-260]. This result is consistent with the composition of the initial black mass treated. The SEM micrograph (Figure 5b) reveals a heterogeneous surface topography, characterized by irregular, micron-sized particulate agglomerates anchored onto larger, smooth carbonaceous sheets (graphite matrix).

Table 3. Chemical compositions of (a) the thermally treated, and (b) the water-leached black mass.

Element	wt.%	
	(a)	(b)
Al	1.039	1.960
B	0.028	0.146
Ba	0.000	<0.001
Bi	n.d.	<LD
Ca	0.007	0.013
Cd	<LD	<LD
Co	0.102	0.199
Cr	0.008	0.014
Cu	0.638	1.042
Fe	0.057	0.115
K	0.009	0.004
Li	6.292	1.431
Mg	0.002	0.020
Mn	0.071	0.031
Mo	<LD	<LD
Na	0.062	0.159
Ni	0.470	0.822
P	0.028	0.055
Pb	<LD	0.001
S	1.291	1.426
Sb	<LD	<LD
Si	0.034	0.047
Sn	0.007	0.011
Sr	<LD	<LD
Ta	<LD	<LD
Ti	0.001	0.002
V	<LD	<LD
Zn	0.033	0.040

LD: Limit of detection.

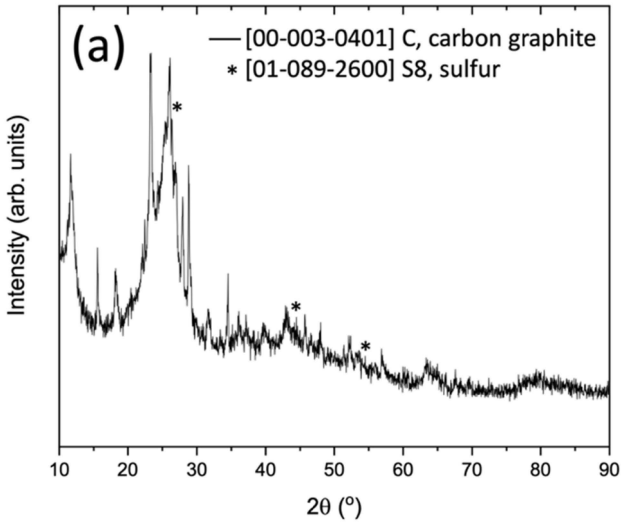

Figure 5. *Cont.*

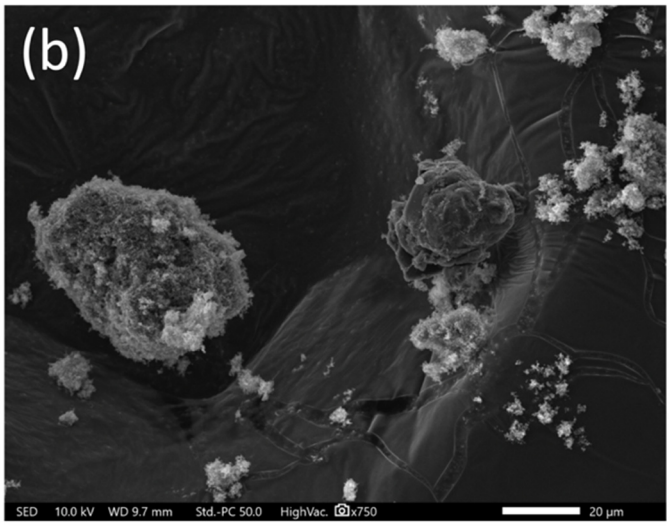

Figure 5. (**a**) XRD pattern and (**b**) SEM image and EDX analysis of the obtained insoluble product.

The chemical composition of the aqueous fraction was also determined from ICP-OES measurements, as shown in Table 4. Lithium was identified as the predominant species within the recovered liquid fraction. This high concentration demonstrates that the lithium was efficiently recovered in the liquid fraction, confirming that it remained as a highly water-soluble phase (such as residual LiCl) within the porous carbon host after the thermal treatment step. Furthermore, a significant sulfur concentration was detected, indicating partial dissolution of the sulfur-bearing subproducts generated during Li-$SOCl_2$ battery discharge, and subsequent thermal treatment. Finally, impurities exhibited minimal dissolution, remaining in minor trace quantities.

Table 4. Chemical composition of the aqueous fraction obtained after the water-leaching step.

Element	Concentration (mg/L)
Al	24.381
B	3.359
Ba	0.030
Bi	<LD
Ca	3.944
Cd	0.026
Co	46.658
Cr	<LD
Cu	35.015
Fe	<LD
K	11.686
Li	12,896.200
Mg	0.699
Mn	115.796
Mo	<LD
Na	68.037
Ni	125.820
P	<LD
Pb	<LD
S	1199.660
Sb	<LD
Si	3.055
Sn	0.677

Table 4. *Cont.*

Element	Concentration (mg/L)
Sr	0.090
Ta	0.096
Ti	<LD
V	<LD
Zn	32.965

LD: Limit of detection.

3.3. Lithium Recovery

Unlike oxide-based lithium-ion battery black masses, which are reduced by the carbothermic reduction reaction, typically leading to the formation of either Li_2CO_3 or Li_2O, lithium in spent Li-$SOCl_2$ batteries is in a different chemical form, as it is chiefly found in the discharged form as LiCl. Therefore, thermal treatment is not expected to reduce Li^+ to metallic lithium. Instead, it is anticipated that it will only result in the decomposition of sulfur-based compounds and some of the residual electrolyte, with lithium remaining in its ionic state principally as water-soluble LiCl. This interpretation is consistent with the high lithium extraction achieved after the water-leaching in this study.

Lithium recovery from the leached solution using a precipitation approach was investigated for the selective precipitation of lithium carbonate. This process is based on the reaction between Li^+ ions in dissolution and carbonate ions supplied by a carbonating reagent.

Among the reagents evaluated, ammonium carbonate ($(NH_4)_2CO_3$) was first selected due to its ability to promote $LiCO_3$ formation (Equation (4)) while avoiding the incorporation of foreign cations into the crystal lattice, thus enabling the production of a high-purity lithium compound [18].

$$2Li^+(aq) + (NH_4)_2CO_3(s) \rightarrow Li_2CO_3 \downarrow + 2NH_4^+(aq) \quad (4)$$

Therefore, different experimental conditions were assessed (summarized in Table 5):

Table 5. Experimental conditions and lithium recovery efficiencies of the different precipitation routes.

Route	Precipitation Step	pH Adjustment	Remarks	Lithium Recovery (%)
(1)	Stoichiometric amount of $(NH_4)_2CO_3$ slowly added	Not required	Direct precipitation from solution	38
(2)	$(NH_4)_2CO_3$:Li = 2:1 (molar ratio)	Not required	Controlled precipitation via carbonate excess	65
(3)	$(NH_4)_2CO_3$:Li = 2:1 (molar ratio)	Basified with NaOH to pH = 11 before carbonate addition	Two-step process: basification + precipitation step	68

(1) For the lithium solution, a stoichiometric amount of ammonium carbonate was slowly added to the Li solution. This precipitation was carried out with slight heating to prevent the solubilization of lithium carbonate. (2) For the lithium solution, ammonium carbonate was slowly added at a molar ratio of 2:1 (ammonium carbonate:lithium). This precipitation was also carried out with slight heating to prevent solubilization of the lithium carbonate. (3) The initial lithium solution was basified by the addition of NaOH until a pH of 11 was reached. To the basified solution, ammonium carbonate was slowly added at a

molar ratio of 2:1 (2:1 carbonate: lithium). This precipitation was carried out with slight heating to promote the formation of lithium carbonate.

The obtained results from the precipitation tests are also shown in Table 5 in terms of lithium recovery efficiency (%). This percentage was calculated based on the stoichiometric relationship between the lithium recovered as Li_2CO_3, and the initial lithium concentration present in the solution. As indicated, the lowest lithium recovery yield (38%) was obtained under route (1) when utilizing a strictly stoichiometric amount of $(NH_4)_2CO_3$. This poor performance is related to the relatively high solubility of lithium carbonate in aqueous media at ambient temperature, which prevents complete precipitation under equimolar conditions. In contrast, efficiency enhancement was achieved under route (2) by increasing the $(NH_4)_2CO_3$ molar ratio to 2:1, leading to lithium recovery yield of up to 65%. This marked improvement can be attributed to the common-ion effect, whereby the excess carbonate ions (CO_3^{2-}) force more dissolved lithium to precipitate, which minimizes the amount of lithium that remains dissolved. The maximum recovery yield (68% lithium recovery) using $(NH_4)_2CO_3$ as the precipitating reagent was achieved via route (3), which combined a 2:1 molar ratio with a basification step previously using NaOH to reach a pH of 11. Although the final recovery efficiencies of routes (2) and (3) appear similar, the alkaline environment in route (3) plays a critical role in preventing the protonation of carbonate ions into bicarbonate (HCO_3^-). At pH below 10, the concentration of active (CO_3^{2-}) ions decreases due to the equilibrium with (HCO_3^-), which forms highly soluble lithium bicarbonate ($LiHCO_3$) and hinders the final recovery. Thus, increasing the pH to 11 kept the carbonate species fully deprotonated, maximizing the availability of (CO_3^{2-}) ions to react with the remaining Li^+ ions.

Although alkaline conditions and an increased ammonium carbonate dosage theoretically seem to promote lithium carbonate precipitation, the relatively low recovery efficiency could be attributed to the thermal instability of the precipitating reagent.

Based on the optimal conditions obtained, further precipitation experiments were conducted to optimize lithium recovery from the leach solution. According to previous studies, ammonium carbonate gradually decomposes into water vapor, carbon dioxide, and ammonia at 58 °C [19,20], according to Equation (5). Therefore, lithium precipitation may not be complete even with excess ammonium carbonate added.

$$(NH_4)_2CO_3 \rightarrow 2NH_3 + H_2O + CO_2 \quad (5)$$

In addition, previous studies have investigated the addition of non-aqueous solvents to lithium precipitation. The presence of a non-aqueous solvent in the medium results in a decrease in the dielectric constant of the medium (water ≈ 80; ethanol ≈ 25) and less solvation of the ions, which causes a decrease in the solubility of Li_2CO_3 and therefore greater supersaturation and precipitation [18].

Finally, previous studies have shown that precipitation efficiency is higher at higher concentrations of lithium in the initial solution because a more concentrated solution facilitates the formation of an insoluble solid through interactions with the precipitating agent [21,22]. Therefore, the initial lithium solution was concentrated 2.5-fold. After that, the lithium concentrate solution was again basified using sodium hydroxide at a pH higher than 11 and selectively precipitated using a stoichiometric amount of sodium hydroxide with light heating. Finally, the obtained solid was filtered, and the corresponding liquid and solid fractions were analyzed.

Thus, different experimental conditions were assessed (summarized in Table 6):

Table 6. Experimental conditions and lithium recovery efficiencies for the different precipitation routes.

Route	Precipitation Step	Remarks	Lithium Recovery (%)
(4)	Na_2CO_3:Li = 2:1 (molar ratio)	Controlled precipitation via carbonate excess	80
(5)	Na_2CO_3:Li = 2:1 (molar ratio) + EtOH	Controlled precipitation via carbonate excess with dielectric constant modification	88
(6)	Preconcentration + Na_2CO_3:Li = 2:1 (molar ratio) + EtOH	Two-step process: preconcentration + precipitation step	≈100

Routes (4) and (5) evaluate the use of sodium carbonate (Na_2CO_3) at a 2:1 molar ratio, substituting the previously tested carbonating agent. Specifically, route (5) incorporates ethanol (EtOH) to decrease the solubility of lithium carbonate via dielectric constant modification of the aqueous medium. Additionally, route (6) evaluates a two-step process that combines an initial stage to concentrate the solution, followed by precipitation using Na_2CO_3 with the addition of EtOH as an antisolvent.

As can be observed, route (4) yielded a recovery of 80%, indicating the effectiveness of using Na_2CO_3 under excess conditions to promote precipitation equilibrium. In route (5), this value was increased to 88% due to the addition of ethanol, which reduces the lithium carbonate solubility by changing the dielectric constant of the aqueous phase. Finally, route (6) obtained nearly complete lithium recovery (near 100%). This excellent performance is attributed to the synergistic effect of the initial solution preconcentration step and the antisolvent-assisted precipitation step. This two-step configuration is the best strategy to maximize efficiency.

3.4. Lithium Carbonate Characterization

Table 7 shows the chemical composition of both lithium carbonate samples obtained under the optimal conditions determined by ICP-OES. Lithium is the predominant element in both samples, with concentrations of 20.845 wt.% and 19.265 wt.% for the Li_2CO_3 obtained using ammonium carbonate and sodium carbonate, respectively. These values are close to the theoretical lithium content of pure Li_2CO_3 (i.e., 18.79 wt.%). Regarding impurities, both samples exhibited a high degree of purity, as the remaining elements were present at concentrations below 0.1 wt.%. Sulfur was the main impurity in both samples, although at concentrations of 0.051 wt.% and 0.034 wt.%, respectively.

Table 7. Chemical compositions of the final lithium carbonates obtained using (a) ammonium carbonate and (b) sodium carbonate through optimal conditions.

Element	wt.%	
	(a)	(b)
Al	0.004	0.001
B	0.003	0.002
Ca	0.023	<LD
Co	0.005	<LD
Cu	0.001	<LD
K	0.005	0.004
Li	20.845	19.265

Table 7. *Cont.*

Element	wt.%	
	(a)	(b)
Mg	0.005	0.001
Mn	0.013	<LD
Na	0.007	0.083
Ni	0.001	<LD
S	0.051	0.034
Sn	0.001	0.001
Zn	0.003	0.001

The XRD patterns of the final solids obtained under the optimal conditions using the different precipitating agents are shown in Figure 6a,b. All diffraction maxima can be attributed to the lithium carbonate phase (Li_2CO_3 PDF-2 no 01-087-0728). Within the sensitivity of the measurements, no more maxima were detected. In addition, SEM micrographs for the recovered lithium carbonates are also shown in Figure 6c,d, where particle agglomerates can be observed.

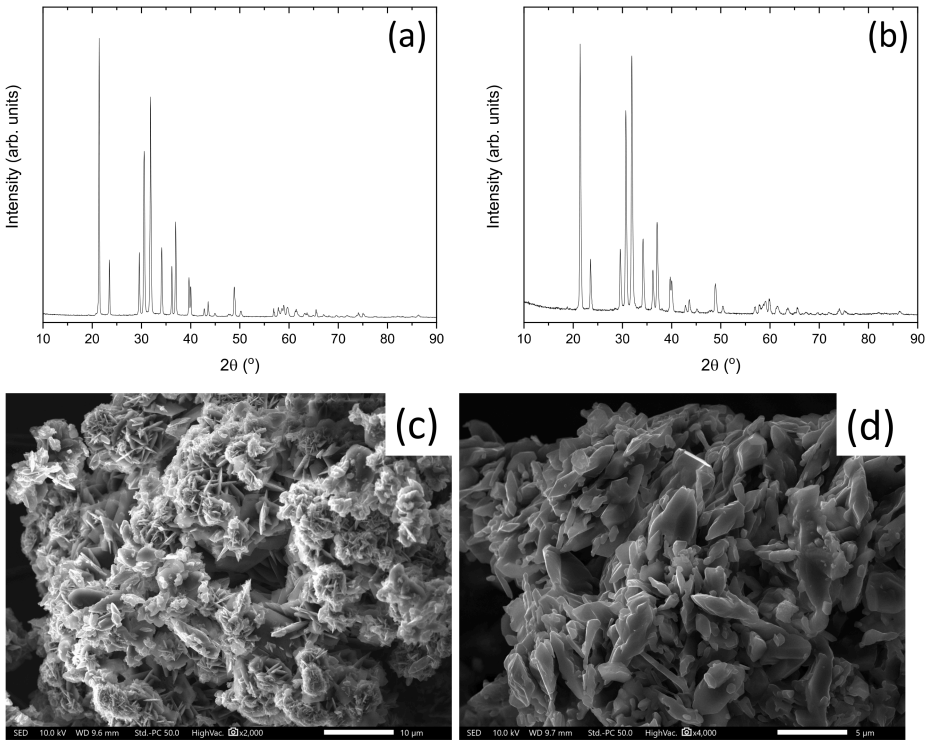

Figure 6. XRD patterns and SEM micrographs of the obtained final products obtained via (**a**,**c**) route (3), and (**b**,**d**) route (6).

Finally, the overall lithium mass balance and the flow diagram for the optimized recycling route (Route 6), starting from the recovered black mass from spent Li-$SOCl_2$ batteries (100% Li baseline), are detailed in Figure 7. During the thermal treatment step at 500 °C for 2 h, a 7 wt.% Li loss occurred via thermal volatilization, yielding a thermally treated solid containing 93 wt.% Li of the initial lithium. Subsequent water leaching and filtration achieved 85 wt.% Li extraction efficiency, transferring 79 wt.% Li of the initial lithium into the aqueous filtrate while leaving 13.95 wt.% Li unextracted in the solid residue. Finally, antisolvent-assisted precipitation from the preconcentrated, basified solution using

Na_2CO_3 and EtOH achieved virtually complete lithium recovery, resulting in an overall global lithium recovery yield of 78.5 wt.% Li as high-purity Li_2CO_3.

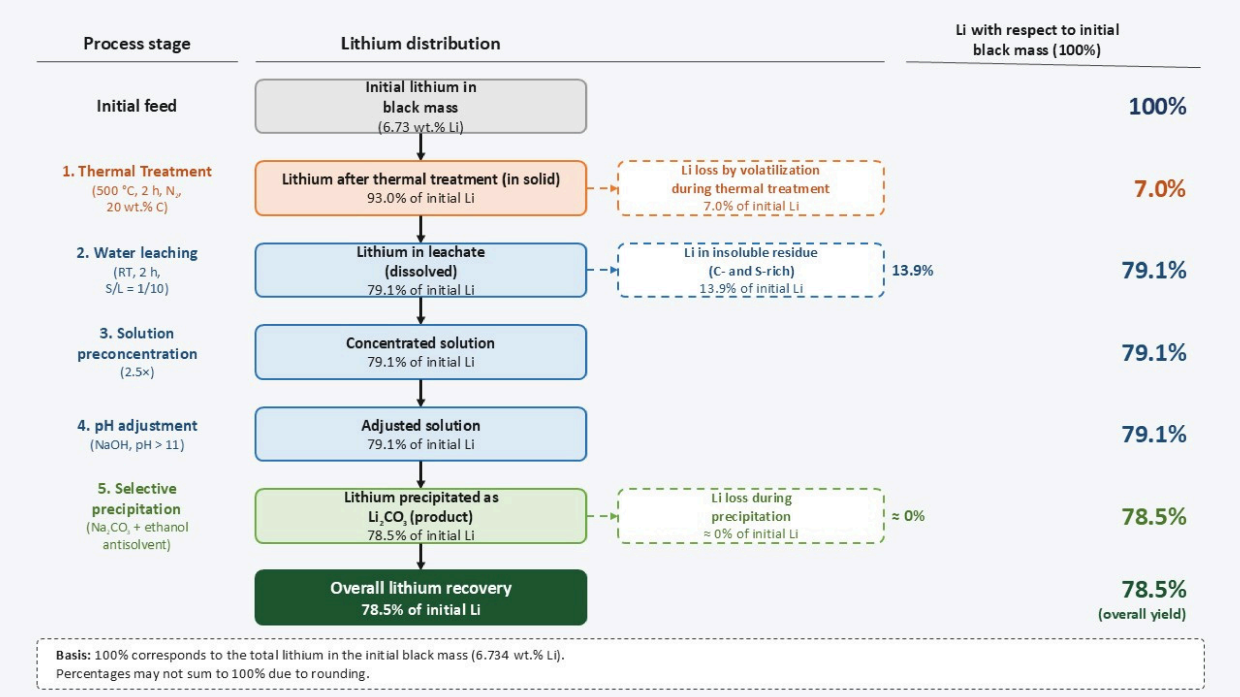

Figure 7. Schematic flowsheet and lithium mass balance of the optimized recycling route (route 6) applied to spent Li-$SOCl_2$ battery black mass. Percentages indicate lithium distribution and loss at each process stage, normalized to 100% lithium in the initial black mass.

4. Conclusions

The present study demonstrates the technical feasibility of recovering lithium from spent Li-$SOCl_2$ primary batteries through an integrated thermal–hydrometallurgical process. The thermal treatment was identified as a critical operation because excessive temperature promotes lithium volatilization. Treatment at 500 °C for 2 h limited lithium loss to approximately 7%, whereas increasing the temperature to 850 °C resulted in substantially higher loss. The subsequent water-leaching step demonstrated that the chemical form of lithium in this battery chemistry can be advantageously exploited for selective recovery. Approximately 85% of the lithium remaining after thermal treatment was transferred to the aqueous phase, while most of the metallic impurities remained in the solid residue. The precipitation experiments further showed that lithium recovery is governed not only by the choice of precipitating agent but also by the chemical conditions of the solution. Although ammonium carbonate enabled the selective formation of high-purity Li_2CO_3, increasing the carbonate excess and adjusting the solution to alkaline conditions resulted in only moderate lithium recovery, reaching 68%. In comparison, the use of sodium carbonate, combined with solution preconcentration and ethanol-assisted precipitation, enabled almost complete recovery of the dissolved lithium. This demonstrates the importance of controlling lithium concentration and Li_2CO_3 solubility to maximize precipitation efficiency. Overall, the proposed thermal–hydrometallurgical process achieved an overall lithium recovery yield of 78.5% from the initial black mass feed and produced high-purity lithium carbonate. Beyond the recovery performance itself, the work highlights the possibility of establishing dedicated recycling routes for Li-$SOCl_2$ batteries, a hazardous and still underexplored waste stream. The approach contributes to the diversification of secondary lithium sources and supports circular economy strategies aimed at reducing dependence

on primary lithium resources. Future research should focus on scaling up the process, improving lithium recovery during the thermal stage, and investigating the valorization of the remaining sulfur- and carbon-rich solid residues to further enhance overall process sustainability.

Author Contributions: L.A.: Writing—review and editing, Writing—original draft, Validation, Methodology, Investigation, Formal analysis, Data curation. O.R.-L.: Writing—review and editing, Validation. F.A.L.: Writing—review and editing, Validation, Resources, Investigation, Supervision, Conceptualization. All authors have read and agreed to the published version of the manuscript.

Funding: This work was supported by the European Union's Horizon Europe Programme (HORIZON-KDT-JU-2022-2-RIA) under Project EECONE (Grant Agreement No. 101112065), and by the Spanish Agencia Estatal de Investigación under Project PCI2023-143382.

Data Availability Statement: The data presented in this study are available on request from the corresponding author (please specify the reason for restriction, e.g., the data are not publicly available due to privacy or ethical restrictions).

Acknowledgments: Microsoft Copilot M365 (USA) was used as an AI-assisted tool to create the graphical abstract. The tool was used only for visual generation, and all content was reviewed and validated by the authors.

Conflicts of Interest: The authors declare no conflicts of interest.

References

1. Ngoy, K.R.; Lukong, V.T.; Yoro, K.O.; Makambo, J.B.; Chukwuati, N.C.; Ibegbulam, C.; Eterigho-Ikelegbe, O.; Ukoba, K.; Jen, T.-C. Lithium-Ion Batteries and the Future of Sustainable Energy: A Comprehensive Review. *Renew. Sustain. Energy Rev.* **2025**, *223*, 115971. [CrossRef]
2. Lu, J.; Chen, S.; Li, Y.; Du, X.; Shi, W.; Lin, M. Primary Amine-Mediated Single-Step Extraction: A Sustainable Strategy for High-Efficiency Lithium Recovery from Waste NMC Lithium-Ion Batteries. *Desalination* **2026**, *622*, 119771. [CrossRef]
3. Flexer, V.; Baspineiro, C.F.; Galli, C.I. Lithium Recovery from Brines: A Vital Raw Material for Green Energies with a Potential Environmental Impact in Its Mining and Processing. *Sci. Total Environ.* **2018**, *639*, 1188–1204. [CrossRef]
4. Vikström, H.; Davidsson, S.; Höök, M. Lithium Availability and Future Production Outlooks. *Appl. Energy* **2013**, *110*, 252–266. [CrossRef]
5. Hao, J.; Wang, Y.; Wu, Y.; Guo, F. Metal Recovery from Waste Printed Circuit Boards: A Review for Current Status and Perspectives. *Resour. Conserv. Recycl.* **2020**, *157*, 104787. [CrossRef]
6. Gaines, L. The Future of Automotive Lithium-Ion Battery Recycling: Charting a Sustainable Course. *Sustain. Mater. Technol.* **2014**, *1–2*, 2–7. [CrossRef]
7. Jiang, H.; Yang, Y.; Sun, S.; Yu, J. Adsorption of Lithium Ions on Lithium-aluminum Hydroxides: Equilibrium and Kinetics. *Can. J. Chem. Eng.* **2020**, *98*, 544–555. [CrossRef]
8. Li, H.; Zhang, D.; Qian, H.; Chen, R.; Cao, Y.; Ai, X.; Wu, J. Li-$SOCl_2$ Batteries: Current Status, Practical Challenges, and Future Perspectives. *J. Energy Chem.* **2026**, *113*, 365–401. [CrossRef]
9. Lai, X.; Chen, Q.; Tang, X.; Zhou, Y.; Gao, F.; Guo, Y.; Bhagat, R.; Zheng, Y. Critical Review of Life Cycle Assessment of Lithium-Ion Batteries for Electric Vehicles: A Lifespan Perspective. *eTransportation* **2022**, *12*, 100169. [CrossRef]
10. Top, S.; Kursunoglu, S.; Altiner, M. A Comprehensive Review on the Extraction and Recovery of Lithium from Primary and Secondary Sources: Advances toward Battery-grade Materials. *Can. J. Chem. Eng.* **2026**, *104*, 2573–2596. [CrossRef]
11. Available online: https://www.epa.gov/hw/lithium-ion-battery-recycling-frequently-asked-questions (accessed on 21 April 2026).
12. Hu, H.; Guo, X.; Yang, L.; Wu, Y.; Yang, G.; Luo, X. Adsorption Materials toward Highly-Efficient Lithium Extraction from Non-Conventional Lithium Sources. *Adv. Mater.* **2025**, *37*, e2506055. [CrossRef]
13. Sun, Y.; Qin, X.; Li, L.; Zhang, Y.; Zhang, J.; Qi, J. The Impact of Temperature on the Performance and Reliability of Li/$SOCl_2$ Batteries. *Energies* **2024**, *17*, 3063. [CrossRef]
14. Schlaikjer, C.R.; Goebel, F.; Marincic, N. Discharge Reaction Mechanisms in Li/$SOCl_2$ Cells. *J. Electrochem. Soc.* **1979**, *126*, 513–522. [CrossRef]
15. Jeon, T.-J.; Wang, J.-P. Preparation and Recovery Behavior of Lithium Chloride (LiCl) from Lithium Iron Phosphate ($LiFePO_4$) Cathode Active Materials via Hydrogen Reduction and $CaCl_2$-Assisted Thermal Chlorination. *Materials* **2026**, *19*, 1474. [CrossRef]

16. Alcaraz, L.; Rodríguez-Largo, O.; Barquero-Carmona, G.; López, F.A. Recovery of Lithium from Spent NMC Batteries through Water Leaching, Carbothermic Reduction, and Evaporative Crystallization Process. *J. Power Sources* **2024**, *619*, 235215. [CrossRef]
17. Qu, G.; Wei, Y.; Liu, C.; Yao, S.; Zhou, S.; Li, B. Efficient Separation and Recovery of Lithium through Volatilization in the Recycling Process of Spent Lithium-Ion Batteries. *Waste Manag.* **2022**, *150*, 66–74. [CrossRef]
18. Nguyen, T.T.H.; Lee, M.S. Comparison of Li(I) Precipitation from the Leaching Solution of the Dust from Spent Lithium-Ion Batteries Treatment between Sodium Carbonate and Ammonium Carbonate. *Resour. Recycl.* **2022**, *31*, 34–41. [CrossRef]
19. Wang, F.; Song, N.; Xia, X.; Chen, X. Experimental Investigation on Transpiration Cooling of Ammonium Carbonate in Porous Composite Structure at High-Temperature. *Appl. Therm. Eng.* **2024**, *249*, 123292. [CrossRef]
20. Haynes, W.M.; Lide, D.R.; Bruno, T.J. *CRC Handbook of Chemistry and Physics*, 97th ed.; CRC Press: Cleveland, OH, USA, 2016.
21. Garcia, L.V.; Ho, Y.-C.; Myo Thant, M.M.; Han, D.S.; Lim, J.W. Lithium in a Sustainable Circular Economy: A Comprehensive Review. *Processes* **2023**, *11*, 418. [CrossRef]
22. Mazurek, K.; Weidner, E.; Drużyński, S.; Ciesielczyk, F.; Kiełkowska, U.; Wróbel-Kaszanek, A.; Jesionowski, T. Lanthanum Enriched TiO_2-ZrO_2 Hybrid Material with Tailored Physicochemical Properties Dedicated to Separation of Lithium and Cobalt(II) Raising from the Hydrometallurgical Stage of the Recycling Process of Lithium-Ion Batteries. *Hydrometallurgy* **2020**, *197*, 105448. [CrossRef]